HAL
open science

Numerical scheme for kinetic transport equation with internal state

Nicolas Vauchelet, Shugo Yasuda

To cite this version:

Nicolas Vauchelet, Shugo Yasuda. Numerical scheme for kinetic transport equation with internal state. Multiscale Modeling and Simulation: A SIAM Interdisciplinary Journal, 2021, 19 (1), pp.18-27. 10.1137/20m134441x . hal-02861713

HAL Id: hal-02861713

https://hal.science/hal-02861713v1

Submitted on 9 Jun 2020

HAL is a multi-disciplinary open access archive for the deposit and dissemination of scientific research documents, whether they are published or not. The documents may come from teaching and research institutions in France or abroad, or from public or private research centers.

L'archive ouverte pluridisciplinaire **HAL**, est destinée au dépôt et à la diffusion de documents scientifiques de niveau recherche, publiés ou non, émanant des établissements d'enseignement et de recherche français ou étrangers, des laboratoires publics ou privés.

Numerical scheme for kinetic transport equation with internal state*

Nicolas Vauchelet† Shugo Yasuda‡

June 9, 2020

Abstract

We investigate the numerical discretization of a two-stream kinetic system with an internal state, such system has been introduced to model the motion of cells by chemotaxis. This internal state models the intracellular methylation level. It adds a variable in the mathematical model, which makes it more challenging to simulate numerically. Moreover, it has been shown that the macroscopic or mesoscopic quantities computed from this system converge to the Keller-Segel system at diffusive scaling or to the velocity-jump kinetic system for chemotaxis at hyperbolic scaling. Then we pay attention to propose numerical schemes uniformly accurate with respect to the scaling parameter. We show that these schemes converge to some limiting schemes which are consistent with the limiting macroscopic or kinetic system. This study is illustrated with some numerical simulations and comparisons with Monte Carlo simulations.

Keywords: Asymptotic-preserving scheme, chemotaxis, kinetic-transport model with internal state, well-balanced scheme.

AMS Classification: 65M08, 65N08, 65M12, 92C17.

1 Introduction

Kinetic equations are by now widely used to model the motion of bacteria by so-called 'run-and-tumble' process, i.e. an alternance of forward-moving runs with reorienting tumbles. In a simple mathematical model, bacteria respond to a given external chemical signal only by modulating their probability to tumble. Then, the motion of bacteria may be described by the dynamics of their distribution function, which corresponds to the probability to find a bacteria at time t with position x and velocity v. This mathematical approach has been introduced in [15] and has attracted the attention of many mathematical works, in particular it has been shown that Keller-Segel equations may be derived at diffusive scaling (see e.g. [16, 3, 2, 11] and references therein).

Actually, the response of bacteria to signal changes is governed by a sophisticated chemotactic signal transduction pathway. It involves a rapid response of the cell to the external signal change called 'excitation', and a slow 'adaptation' which allows the cell to subtract out the background signal. In order to describe the multiscale mechanism between the intracellular chemo-sensory system and the individual and collective motions of bacteria, more elaborated kinetic models have been proposed. In [3, 4], a cell-based model which incorporates a linear cartoon description of the excitation

*This work was supported by Japan-France Integrated action Program (SAKURA), Grant number JPJSBP120193219.

†Université Sorbonne Paris Nord, Laboratoire Analyse, Géométrie et Applications, LAGA, CNRS UMR 7539, F-93430, Villetaneuse, France. (email : vauchelet@math.univ-paris13.fr).

‡University of Hyogo, Graduate School of Simulation Studies, Kobe 650-0047, Japan (email : yasuda@sim.u-hyogo.ac.jp).

and adaptation response of a cell has been introduced. The signal transduction pathway has been studied in e.g. [10, 17]. We refer to [17, 24, 28, 26] where the case of bacteria *E. coli* and the link between cell-based models and continuum models have been extensively studied.

In this paper, we consider the simplest description of the biochemical pathways, in which a single additional variable $m \geq 0$, which represents the intracellular methylation level, is used. The methylation has an equilibrium level M, depending on time t and position x. Using $F(m, M)$ as the adaptation rate, the intracellular adaptation dynamics is governed by a differential equation

$$\frac{dm}{dt} = F(m, M(t, x)).$$

In order to model the dynamics of a population of bacteria, the following pathway-based kinetic-transport model has been proposed in [3, 22]. Let $q(t, x, v, m)$ be the probability density function of bacteria at time t, position $x \in \mathbb{R}^d$, moving at velocity $v \in \mathbb{V}$, where $\mathbb{V}$ is a bounded domain of $\mathbb{R}^d$, and methylation level $m > 0$. We have

$$\begin{cases} \partial_t q + v \cdot \nabla_x q + \partial_m [F(m, M) q] = \mathcal{Q}[m, M](q), \\ q(x, v, m = 0, t) = 0. \end{cases} \tag{1.1}$$

The 'run' phase is modelled by the transport term in x, whereas the evolution of the methylation level is modelled by the m-derivative. The 'tumble' phase is described in the right hand side by the tumbling operator $\mathcal{Q}[m, M](q)$. It is given by

$$\mathcal{Q}[m, M](q) = \frac{1}{\|\mathbb{V}\|} \int_{\mathbb{V}} \left[\lambda(m, M, v, v') q(t, x, v', m) - \lambda(m, M, v', v) q(t, x, v, m) \right] dv', \tag{1.2}$$

where $\lambda(m, M, v, v')$ denotes the methylation dependent tumbling frequency from v' to v. Departing from such pathway-based kinetic equation several authors (see [3, 4, 2, 25, 21, 26, 23, 19]) developed the asymptotic theory which allows to recover, in the diffusion limit, macroscopic equations as the Keller-Segel (KS) or the flux-limited Keller-Segel (FLKS) system which governs the dynamics of the macroscopic quantities depending only on t and x. In [18], the authors show that, at hyperbolic scaling, the above pathway-based kinetic equation converges to the classical velocity jump kinetic equation for mesoscopic quantities depending on t, x, and v.

For *E. coli* chemotaxis, it may be assumed that the tumbling frequency λ in (1.2) depends only on $M - m$ [22] : $\lambda(m, M, v, v') = \lambda_0 \Lambda(\frac{M-m}{\delta})$, where $\lambda_0 > 0$ is the mean tumbling frequency and $\delta > 0$ is the stiffness of the chemotactic response. Moreover, we consider the linear model

$$\frac{dm}{dt} = F(m, M) = \frac{1}{\tau}(M - m),$$

where $\tau > 0$ is the characteristic time of adaptation. The equilibrium level M is a function of extra-cellular chemical concentration and is assumed to be independent of time. Usually, it has a logarithmic dependancy as it has been experimentally evidenced for *E. coli* in [14], which allows to consider that $\nabla_x M$ is uniform in space in exponential environment. We denote $G \in \mathbb{R}^d$ the constant vector $G = \nabla_x M$. Then, we introduce the new variable $y = \frac{M(x)-m}{\delta}$, and the unknown $p(t, x, v, y) = q(t, x, v, m)$. After this change of variable and introducing a time scaling parameter σ, equation (1.1) rewrites (see [18, 19])

$$\sigma \partial_t p(t, x, v, y) + v \cdot \nabla_x p + \partial_y \left((v \cdot \frac{G}{\delta} - \frac{y}{\tau}) p \right) = \lambda_0 \Lambda(y)(\langle p \rangle - p). \tag{1.3}$$

An asymptotic analysis of Eq. (1.3) depending on the scalings of λ_0^{-1}, δ, σ, and τ may lead to various models. In [19], several scalings have been investigated depending on the relative magnitude order of $\lambda_0^{-1} = \varepsilon$, $\delta = \tau$, and σ. In particular, the authors recover macroscopic flux-limited Keller-Segel models or Keller-Segel models as $\varepsilon \to 0$ when $\delta = \tau = \varepsilon$ and $\sigma = \varepsilon^2$, when $\delta = \tau = \varepsilon^2$, $\sigma = \varepsilon$, and when $\delta = \tau = 1$, $\sigma = \varepsilon$. In [18], the authors consider the hyperbolic case $\lambda_0^{-1} = 1$ and $\delta = \tau = \varepsilon$ for which the limiting model is the kinetic 'run-and-tumble' model. Let us mention that these limits are singular in the sense that the distribution function converges to Dirac deltas.

In order to further illustrate those asymptotic behaviors numerically and elucidate the complicated multiscale mechanism between the intra-cellular pathway dynamics and the collective motions of bacteria, one needs an accurate and efficient numerical method which can address the asymptotic limits. This paper is devoted to the numerical discretization and simulation of such kinetic system with internal variable (1.3). In order to simplify the study and facilitate the presentation of the computations, we consider the problem in one dimensional spatial domain and assume that $v \in \{-1, 1\}$. We denote by $p^{\varepsilon,+}(t, x, y)$ and $p^{\varepsilon,-}(t, x, y)$ the unknowns, depending on ε, of our problem. In this one dimensional setting with $\delta = \tau$, equation (1.3) rewrites

$$\sigma \partial_t p^{\varepsilon,\pm} \pm \partial_x p^{\varepsilon,\pm} + \frac{1}{\tau} \partial_y((\pm G - y) p^{\varepsilon,\pm}) = \pm \lambda_0 \frac{\Lambda(y)}{2} (p^{\varepsilon,-} - p^{\varepsilon,+}). \tag{1.4}$$

This system is complemented with some initial data $p^{\varepsilon,\pm}(t = 0, y)$. In this work, we would like to propose numerical schemes for (1.4) which are able to deal with the diffusive limit ($\sigma = \lambda_0^{-1} = \varepsilon \ll 1 = \tau$) and the hyperbolic limit ($\sigma = \lambda_0 = 1, \tau = \varepsilon \ll 1$). This is the so-called asymptotic preserving (AP) property [7, 13]. There are several challenging issues in doing so. As already mentionned, one difficulty is due to the extra variable y, then usual AP numerical schemes for kinetic equations may not be directly applied. Another difficulty is that the distribution function has a singular limit when $\varepsilon \to 0$ since it converges to Dirac deltas (see [18, 19]). To overcome these difficulties, we follow the approach in [5], which proposes accurate numerical schemes preserving stationary states, and we couple it with a projection step which allows us to capture the Dirac deltas.

The paper is organized as follows. In Section 2.1, we investigate the numerical discretization of system (1.4) at diffusive scaling. We propose a numerical scheme having the so-called asymptotic preserving property. Section 3 deals with the hyperbolic scaling. Although we follow the same idea as for the diffusive scaling, the scheme should be adapted to this scaling, as it is emphasized in §3.3. Numerical illustrations are proposed in Section 4 and compared with a Monte Carlo (MC) scheme. This paper ends with a conclusion. Finally, an appendix gathers a useful technical computation and a presentation of the MC scheme used for comparison.

2 Diffusive scaling

2.1 System at diffusive scaling

We first consider system (1.4) at the diffusive limit $\sigma = \lambda_0^{-1} = \varepsilon, \tau = 1$. We denote $p^{\varepsilon,+}(t, x, y)$, resp. $p^{\varepsilon,-}(t, x, y)$, the distribution function of bacteria at time $t > 0$, with internal state y, going to the positive, resp. negative, direction. Their dynamics is governed by the system :

$$\varepsilon^2 \partial_t p^{\varepsilon,\pm} \pm \varepsilon \partial_x p^{\varepsilon,\pm} + \varepsilon \partial_y((\pm G - y) p^{\varepsilon,\pm}) = \pm \frac{\Lambda(y)}{2} (p^{\varepsilon,-} - p^{\varepsilon,+}). \tag{2.5}$$

We first notice that it has been proved in [19] that when the support of initial data $p^{\varepsilon,\pm}(0, \cdot)$ is included into $[-|G|, |G|]$, then for any $t > 0$ the support of $p^{\varepsilon,\pm}(t, \cdot)$ is also included into $[-|G|, |G|]$.

Thus we will assume that the support in y of the initial data is included into $[-|G|, |G|]$ such that the domain of the internal variable y is $[-|G|, |G|]$.

Before focusing on the numerical discretisation of (2.5), we first explain how to perform formally the diffusive limit $\varepsilon \to 0$ into (2.5). Let us assume formally that $p^{\varepsilon,\pm}$ admit a Hilbert expansion $p^{\varepsilon,\pm} = p_0^{\pm} + \varepsilon p_1^{\pm} + O(\varepsilon^2)$. Letting $\varepsilon \to 0$ in (2.5), we first deduce that $p_0^+ = p_0^- = p_0$. Then, injecting the Hilbert expansion into (2.5) and identifying the term at order 1 in ε, we get

$$\pm\partial_x p_0 + \partial_y((\pm G - y)p_0) = \pm\frac{\Lambda(y)}{2}(p_1^- - p_1^+).$$

Adding these two equations, we deduce $\partial_y(yp_0) = 0$. Hence $p_0(t,x,y) = \bar{p}_0(t,x)\delta_{y=0}$ for some $\bar{p}_0$. We are left with the relation

$$\partial_x p_0 + \partial_y(Gp_0) = \frac{\Lambda(y)}{2}(p_1^- - p_1^+).$$

Therefore, injecting the relation $p_0(t,x,y) = \bar{p}_0(t,x)\delta_{y=0}$, we get

$$p_1^- - p_1^+ = \frac{2}{\Lambda(y)}\partial_x\bar{p}_0\delta_{y=0} + \frac{2G\bar{p}_0}{\Lambda(y)}\delta'_{y=0}.$$

Integrating over y, we deduce

$$\int_{\mathbb{R}}(p_1^- - p_1^+)\,dy = \frac{2}{\Lambda(0)}\partial_x\bar{p}_0 + 2G\bar{p}_0\frac{\Lambda'(0)}{\Lambda(0)^2}. \tag{2.6}$$

Moreover, adding the two equations in (2.5) and letting formally $\varepsilon \to 0$ leads to

$$2\partial_t p_0 + \partial_x(p_1^+ - p_1^-) + \partial_y(G(p_1^+ - p_1^-) - y(p_1^+ + p_1^-)) = 0.$$

Integrating over y and injecting (2.6), we get

$$\partial_t\bar{p}_0 - \partial_x\left(\frac{1}{\Lambda(0)}\partial_x\bar{p}_0 + G\bar{p}_0\frac{\Lambda'(0)}{\Lambda(0)^2}\right) = 0, \tag{2.7}$$

which is the Keller-Segel equation for the density $\bar{p}_0$. This formal computation has been done rigorously in [19].

2.2 A consistent uniform numerical scheme

From above computations, we observe that a difficulty in the design of the numerical scheme is the emergence of Dirac deltas at the diffusive limit. Then, an uniform numerical scheme should be able to captur this Dirac deltas. In order to overcome this difficulty, we consider an approach consisting in two steps:

- In a first step we solve
$$\partial_t p^{\pm} - \frac{1}{\varepsilon}\partial_y(yp^{\pm}) = 0. \tag{2.8}$$
When $\varepsilon \to 0$ this step may be seen as a projection step onto the set of Dirac deltas in $y = 0$ which is the limiting set. Indeed taking $\varepsilon \to 0$ into this equation leads formally to $\partial_y(yp^{\pm}) = 0$ which implies that $p^{\pm}$ are Dirac deltas in $y = 0$. A similar idea has also been used in [6].

- In a second step we consider an uniform discretization of
$$\varepsilon\partial_t p^{\pm} \pm \partial_x p^{\pm} \pm G\partial_y p^{\pm} = \pm\frac{\Lambda(y)}{2\varepsilon}(p^- - p^+). \tag{2.9}$$

More precisely, let us consider a cartesian grid $x_i = i\Delta x$ for $i \in \mathbb{Z}$ and $y_k = k\Delta y$ for $k = -K, \dots, K$ such that $K\Delta y = |G|$. In this paper, to simplify the computations, we assume that $\Delta y = |G|\Delta x$, unless otherwise stated.

In the first step, we discretize (2.8) by an implicit upwind scheme

$$p_{i,k}^{\pm,n+\frac{1}{2}} = p_{i,k}^{\pm,n} - \frac{\Delta t}{\varepsilon \Delta y}\Big(J_{i,k+\frac{1}{2}}^{\pm,n+\frac{1}{2}} - J_{i,k-\frac{1}{2}}^{\pm,n+\frac{1}{2}}\Big), \tag{2.10a}$$

$$J_{i,k+\frac{1}{2}}^{\pm,n+\frac{1}{2}} = (-y_k)^+ p_{i,k}^{\pm,n+\frac{1}{2}} - (-y_{k+1})^- p_{i,k+1}^{\pm,n+\frac{1}{2}}. \tag{2.10b}$$

In this scheme, we use the usual notation $u^+ = \max\{0, u\}$ for the positive part, and $u^- = \max\{0, -u\}$ for the negative part. We impose no-flux boundary conditions at the boundary : $J_{i,K+\frac{1}{2}}^{\pm,n+\frac{1}{2}} = J_{i,-K-\frac{1}{2}}^{\pm,n+\frac{1}{2}} = 0$, for any i.

In the second step, we discretize (2.9) thanks to a well-balanced asymptotic preserving scheme. However, this equation may be considered as a two-dimensional equation with the two directions x and y. In order to be consistent with the asymptotic limit, it is not a good idea to split the directions as it is illustrated in §3.3. Truly two-dimensional well-balanced schemes are not much developed yet. We mention the recent paper [1], and [9] in the particular case of radiative transfer equation. However, the case at hand can be seen as a one dimension problem by introducing a new variable. Indeed, let us denote $q^\pm(t,z) = p^\pm(t, x+z, y+zG)$, then (2.9) rewrites

$$\varepsilon \partial_t q^\pm \pm \partial_z q^\pm = \pm \frac{\Lambda(y+zG)}{2\varepsilon}(p^- - p^+).$$

This latter equation can be discretized following the idea in [7, 8]. We find the numerical scheme

$$\begin{aligned}
q_j^{+,n+1} &= q_j^{+,n+\frac{1}{2}} - \frac{\Delta t}{\varepsilon \Delta x}(q_j^{+,n+1} - q_j^{-,n+1}) + \frac{2\Delta t G}{\Delta x(2\varepsilon G + \bar{\Lambda}_{k-\frac{1}{2}})}(q_{j-1}^{+,n+\frac{1}{2}} - q_j^{-,n+\frac{1}{2}}) \\
q_{j-1}^{-,n+1} &= q_{j-1}^{-,n+\frac{1}{2}} + \frac{\Delta t}{\varepsilon \Delta x}(q_{j-1}^{+,n+1} - q_{j-1}^{-,n+1}) + \frac{2\Delta t G}{\Delta x(2\varepsilon G + \bar{\Lambda}_{k-\frac{1}{2}})}(q_j^{-,n+\frac{1}{2}} - q_{j-1}^{+,n+\frac{1}{2}}),
\end{aligned}$$

where $\bar{\Lambda}_{k-\frac{1}{2}} = \int_{y_{k-1}}^{y_k} \Lambda(y)\, dy$. Coming back to the notation $p^\pm$, it gives, when $G > 0$,

$$\begin{aligned}
p_{i,k}^{+,n+1} &= p_{i,k}^{+,n+\frac{1}{2}} - \frac{\Delta t}{\varepsilon \Delta x}(p_{i,k}^{+,n+1} - p_{i,k}^{-,n+1}) \\
&\quad + \frac{2\Delta t G}{\Delta x(2\varepsilon G + \bar{\Lambda}_{k-\frac{1}{2}})}(p_{i-1,k-1}^{+,n+\frac{1}{2}} - p_{i,k}^{-,n+\frac{1}{2}})
\end{aligned} \tag{2.11a}$$

$$\begin{aligned}
p_{i-1,k-1}^{-,n+1} &= p_{i-1,k-1}^{-,n+\frac{1}{2}} + \frac{\Delta t}{\varepsilon \Delta x}(p_{i-1,k-1}^{+,n+1} - p_{i-1,k-1}^{-,n+1}) \\
&\quad + \frac{2\Delta t G}{\Delta x(2\varepsilon G + \bar{\Lambda}_{k-\frac{1}{2}})}(p_{i,k}^{-,n+\frac{1}{2}} - p_{i-1,k-1}^{+,n+\frac{1}{2}}).
\end{aligned} \tag{2.11b}$$

When $G < 0$, we have

$$p_{i,k}^{+,n+1} = p_{i,k}^{+,n+\frac{1}{2}} - \frac{\Delta t}{\varepsilon \Delta x}(p_{i,k}^{+,n+1} - p_{i,k}^{-,n+1}) + \frac{2\Delta t G}{\Delta x(2\varepsilon G + \bar{\Lambda}_{k+\frac{1}{2}})}(p_{i-1,k+1}^{+,n+\frac{1}{2}} - p_{i,k}^{-,n+\frac{1}{2}}) \tag{2.12a}$$

$$p_{i-1,k+1}^{-,n+1} = p_{i-1,k+1}^{-,n+\frac{1}{2}} + \frac{\Delta t}{\varepsilon \Delta x}(p_{i-1,k+1}^{+,n+1} - p_{i-1,k+1}^{-,n+1}) + \frac{2\Delta t G}{\Delta x(2\varepsilon G + \bar{\Lambda}_{k+\frac{1}{2}})}(p_{i,k}^{-,n+\frac{1}{2}} - p_{i-1,k+1}^{+,n+\frac{1}{2}}). \tag{2.12b}$$

Finally, the resulting numerical scheme is given by (2.10)–(2.11) when $G > 0$, or (2.10)–(2.12) when $G < 0$. We mention that (2.11) and (2.12) are implicit but can be easily solved by inverting a 2-by-2 matrix.

The following Lemma gives some properties for this scheme:

Lemma 2.1 *Let us assume that $\Delta y = |G|\Delta x$, and that $\Lambda \geq \Lambda_{min} > 0$. Let $(p_{i,k}^{\pm,n})_{i,k,n}$ be a sequence defined thanks to scheme* (2.10)–(2.11) *when $G > 0$, or* (2.10)–(2.12) *when $G < 0$. Then, under the condition*

$$\Delta t \leq \frac{1}{2}\Lambda_{min}\Delta x^2, \tag{2.13}$$

the scheme is positive.

Proof. It is well-known that the implicit upwind scheme (2.10) is positive. For the second step, we perform the computations for $G > 0$, the case $G < 0$ being similar. From (2.11), we deduce by inverting the system

$$\begin{aligned}\left(1 + \frac{2\Delta t}{\varepsilon \Delta x}\right) p_{i,k}^{+,n+1} = &\left(1 + \frac{\Delta t}{\varepsilon \Delta x}\right) p_{i,k}^{+,n+\frac{1}{2}} + \frac{\Delta t}{\varepsilon \Delta x} p_{i,k}^{-,n+\frac{1}{2}} \\ &+ \frac{2\Delta t(\Delta t + \varepsilon \Delta x)G}{\varepsilon \Delta x^2(2\varepsilon G + \bar{\Lambda}_{k-\frac{1}{2}})}(p_{i-1,k-1}^{+,n+\frac{1}{2}} - p_{i,k}^{-,n+\frac{1}{2}}) \\ &+ \frac{2\Delta t^2 G}{\varepsilon \Delta x^2(2\varepsilon G + \bar{\Lambda}_{k+\frac{1}{2}})}(p_{i+1,k+1}^{-,n+\frac{1}{2}} - p_{i,k}^{+,n+\frac{1}{2}}),\end{aligned}$$

and

$$\begin{aligned}\left(1 + \frac{2\Delta t}{\varepsilon \Delta x}\right) p_{i,k}^{-,n+1} = &\left(1 + \frac{\Delta t}{\varepsilon \Delta x}\right) p_{i,k}^{-,n+\frac{1}{2}} + \frac{\Delta t}{\varepsilon \Delta x} p_{i,k}^{+,n+\frac{1}{2}} \\ &+ \frac{2\Delta t^2 G}{\varepsilon \Delta x^2(2\varepsilon G + \bar{\Lambda}_{k-\frac{1}{2}})}(p_{i-1,k-1}^{+,n+\frac{1}{2}} - p_{i,k}^{-,n+\frac{1}{2}}) \\ &+ \frac{2\Delta t(\Delta t + \varepsilon \Delta x)G}{\varepsilon \Delta x^2(2\varepsilon G + \bar{\Lambda}_{k+\frac{1}{2}})}(p_{i+1,k+1}^{+,n+\frac{1}{2}} - p_{i,k}^{-,n+\frac{1}{2}}).\end{aligned}$$

Then, this scheme is positive provided all coefficients are positive, which is equivalent to, for all $k \in \{-K, \ldots, K\}$,

$$\frac{2\Delta t G}{\Delta x(2\varepsilon G + \bar{\Lambda}_{k+\frac{1}{2}})} \leq \min\left\{\frac{\Delta t}{\Delta t + \varepsilon \Delta x}, \frac{\Delta t + \varepsilon \Delta x}{\Delta t}\right\} = \frac{\Delta t}{\Delta t + \varepsilon \Delta x}.$$

Since we have by definition $\bar{\Lambda}_{k+\frac{1}{2}} = \int_{y_k}^{y_{k+1}} \Lambda(y)\,dy \geq \Lambda_{\min}\Delta y$, then the above inequality is satisfied for any k provided

$$\frac{2G}{\Delta x(2\varepsilon G + \Lambda_{\min}\Delta y)} \leq \frac{1}{\Delta t + \varepsilon \Delta x},$$

which is equivalent to (2.13) by recalling that $\Delta y = G\Delta x$ for $G > 0$.

□

2.3 Asymptotic scheme

In order to verify the consistency of the scheme at the diffusive limit, we perform the limit $\varepsilon \to 0$ in the above numerical scheme (2.10)–(2.11) when $G > 0$ (the case $G < 0$ being done in a similar way).

Lemma 2.2 *Let the sequence* $(p_{i,k}^{\pm,n+\frac{1}{2}})_{i,k,n}$ *be computed thanks to scheme* (2.10)*. When* $\varepsilon \to 0$*, we have* $p_{i,k}^{\pm,n+\frac{1}{2}} \to \bar{p}_i^{\pm,n}\delta_{k=0}$*, where* $\bar{p}_i^{\pm,n} := \sum_{k=-K}^{K} p_{i,k}^{\pm,n}$.

Proof. Letting $\varepsilon \to 0$ into equation (2.10a), we deduce that $J_{i,k+\frac{1}{2}}^{\pm,n+\frac{1}{2}} = J_{i,k-\frac{1}{2}}^{\pm,n+\frac{1}{2}}$, and for $k = 0$, we have by definition (2.10b) $J_{i,\frac{1}{2}}^{\pm,n+\frac{1}{2}} = 0 = J_{i,-\frac{1}{2}}^{\pm,n+\frac{1}{2}}$. Then, for any $i \in \mathbb{Z}$, $k \in \{-K,\dots,K\}$, $n \in \mathbb{N}$, the limit satisfies $(y_k)^+ p_{i,k}^{\pm,n+\frac{1}{2}} = (y_{k+1})^- p_{i,k+1}^{\pm,n+\frac{1}{2}}$. We deduce that for $k \neq 0$, we have $p_{i,k}^{\pm,n+\frac{1}{2}} = 0$. Thus, for any $i \in \mathbb{Z}$, $k \in \{-K,\dots,K\}$, $n \in \mathbb{N}$, there exists a quantity, denoted $\bar{p}_i^{\pm,n+\frac{1}{2}}$, such that $p_{i,k}^{+,n+\frac{1}{2}} = \bar{p}_i^{\pm,n+\frac{1}{2}}\delta_{k=0}$. Finally, thanks to the no-flux boundary conditions, we deduce that $\bar{p}_i^{\pm,n+\frac{1}{2}} = \sum_k p_{i,k}^{\pm,n+\frac{1}{2}} = \sum_k p_{i,k}^{\pm,n} =: \bar{p}_i^{\pm,n}$. □

We may now pass to the limit into equation (2.11). We have

Lemma 2.3 *Formally, when* $\varepsilon \to 0$ *the sequence* $(p_{i,k}^{\pm,n})_{i,k,n}$ *computed thanks to equations* (2.10)–(2.11) *converges towards* $\frac{1}{2}\rho_i^n\delta_{k=0}$*, where the sequence* $(\rho_i^n)_{i,n}$ *solves the numerical scheme*

$$\rho_i^{n+1} = \rho_i^n + \frac{\Delta t G}{\Delta x}\left(\frac{1}{\bar{\Lambda}_{\frac{1}{2}}}\rho_{i-1}^n - \frac{1}{\bar{\Lambda}_{-\frac{1}{2}}}\rho_i^n + \frac{1}{\bar{\Lambda}_{-\frac{1}{2}}}\rho_{i+1}^n - \frac{1}{\bar{\Lambda}_{\frac{1}{2}}}\rho_i^n\right). \tag{2.14}$$

This scheme is consistent with the Keller-Segel equation (2.7)*.*

Proof. We first observe that when $\varepsilon \to 0$ into (2.11), we have $p_{i,k}^{+,n+1} = p_{i,k}^{-,n+1}$. Hence, for any $n \geq 1$, using also Lemma 2.2, we get that $\lim_{\varepsilon\to 0} p_{i,k}^{+,n+\frac{1}{2}} = \lim_{\varepsilon\to 0} p_{i,k}^{-,n+\frac{1}{2}} = \bar{p}_i^n\delta_{k=0}$.

Moreover, adding the two equations (2.11a) and (2.11b) after a change of index, we get

$$\begin{aligned} p_{i,k}^{+,n+1} + p_{i,k}^{-,n+1} &= p_{i,k}^{+,n+\frac{1}{2}} + p_{i,k}^{-,n+\frac{1}{2}} \\ &+ \frac{2\Delta t G}{\Delta x}\left(\frac{1}{2\varepsilon G + \bar{\Lambda}_{k-\frac{1}{2}}}(p_{i-1,k-1}^{+,n+\frac{1}{2}} - p_{i,k}^{-,n+\frac{1}{2}}) + \frac{1}{2\varepsilon G + \bar{\Lambda}_{k+\frac{1}{2}}}(p_{i+1,k+1}^{-,n+\frac{1}{2}} - p_{i,k}^{+,n+\frac{1}{2}})\right). \end{aligned}$$

Passing into the limit $\varepsilon \to 0$, we get, thanks to Lemma 2.2,

$$(\bar{p}_i^{n+1} + \bar{p}_i^{n+1})\delta_{k=0} = (\bar{p}_i^n + \bar{p}_{i,k}^n)\delta_{k=0}$$
$$+ \frac{2\Delta t G}{\Delta x}\left(\frac{1}{\bar{\Lambda}_{k-\frac{1}{2}}}(\bar{p}_{i-1}^n\delta_{k=1} - \bar{p}_i^n\delta_{k=0}) + \frac{1}{\bar{\Lambda}_{k+\frac{1}{2}}}(\bar{p}_{i+1}^{-,n}\delta_{k=-1} - \bar{p}_i^{+,n}\delta_{k=0})\right).$$

We denote by $\rho_i^n := \sum_{k=-K}^{K}(p_{i,k}^{+,n} + p_{i,k}^{-,n}) = 2\bar{p}_i^n$. By summing over k the latter identity, we obtain (2.14).

We now verify that the limiting scheme (2.14) is consistent with the Keller-Segel equation (2.7).

Recalling that $\bar{\Lambda}_{\frac{1}{2}} = \int_0^{\Delta y}\Lambda(y)\,dy$, we approximate thanks to a trapezoidal rule $\bar{\Lambda}_{\frac{1}{2}} \simeq \frac{\Lambda(0)+\Lambda(\Delta y)}{2}\Delta y \simeq \Lambda(0)\Delta y + \frac{1}{2}\Delta y^2\Lambda'(0)$. Then,

$$\frac{1}{\bar{\Lambda}_{\frac{1}{2}}} \simeq \frac{1}{\Lambda(0)\Delta y(1+\frac{1}{2}\Delta y\frac{\Lambda'(0)}{\Lambda(0)})} \simeq \frac{1}{\Lambda(0)\Delta y}\left(1 - \frac{1}{2}\Delta y\frac{\Lambda'(0)}{\Lambda(0)}\right).$$

By the same token we deduce,

$$\frac{1}{\bar{\Lambda}_{-\frac{1}{2}}} \simeq \frac{1}{\Lambda(0)\Delta y}\left(1 + \frac{1}{2}\Delta y\frac{\Lambda'(0)}{\Lambda(0)}\right).$$

Injecting this approximation into (2.14), recalling the relation $\Delta y = |G|\Delta x$, we deduce

$$\rho_i^{n+1} \simeq \rho_i^n + \frac{\Delta t}{\Delta x^2\Lambda(0)}\left(\rho_{i-1}^n - 2\rho_i^n + \rho_{i+1}^n\right) + \frac{\Delta t G\Lambda'(0)}{2\Delta x(\Lambda(0))^2}\left(\rho_{i+1}^n - \rho_{i-1}^n\right). \tag{2.15}$$

This is a finite difference centered discretization of the Keller-Segel equation (2.7). □

3 Hyperbolic scaling

3.1 System at hyberbolic scaling

In this part, we take $\sigma = \lambda_0 = 1, \tau = \varepsilon$ into (1.4). The system at hyperbolic scaling reads

$$\partial_t p^\pm \pm \partial_x p^\pm + \frac{1}{\varepsilon}\partial_y((\pm G - y)p^\pm) = \pm\frac{\Lambda(y)}{2}(p^- - p^+). \tag{3.16}$$

Formally, when $\varepsilon \to 0$, we obtain $\partial_y((\pm G - y)p^\pm) = 0$. Then, we deduce that $p^+(t,x,y) \to f^+(t,x)\delta_{y=G}$ and $p^+(t,x,y) \to f^-(t,x)\delta_{y=-G}$ as $\varepsilon \to 0$. Then, integrating (3.16) over y, we deduce

$$\partial_t f^\pm \pm \partial_x f^\pm = \pm\frac{1}{2}\big(\Lambda(-G)f^- - \Lambda(G)f^+\big). \tag{3.17}$$

We recover the two stream kinetic system for chemotaxis.

In order to discretize equation (3.16), we proceed in two steps :

- In a first step, we discretize the transport equation

$$\partial_t p^\pm + \frac{1}{\varepsilon}\partial_y((\pm G - y)p^\pm) = 0.$$

As above we use an implicit upwind scheme, which reads, for any $n \in \mathbb{N}$, $i \in \mathbb{Z}$ and $k \in \{-K, \dots, K\}$,

$$p_{i,k}^{\pm,n+\frac{1}{2}} = p_{i,k}^{\pm,n} - \frac{\Delta t}{\varepsilon \Delta y}\Big(J_{i,k+\frac{1}{2}}^{\pm,n+\frac{1}{2}} - J_{i,k-\frac{1}{2}}^{\pm,n+\frac{1}{2}}\Big), \tag{3.18a}$$

$$J_{i,k+\frac{1}{2}}^{\pm,n+\frac{1}{2}} = (\pm G - y_k)^+ p_{i,k}^{\pm,n+\frac{1}{2}} - (\pm G - y_{k+1})^- p_{i,k+1}^{\pm,n+\frac{1}{2}}. \tag{3.18b}$$

We impose no-flux boundary conditions : $J_{i,K+\frac{1}{2}}^{\pm,n+\frac{1}{2}} = J_{i,-K-\frac{1}{2}}^{\pm,n+\frac{1}{2}} = 0$, for any $i \in \mathbb{Z}$.

- In the second step, we discretize

$$\partial_t p^\pm \pm \partial_x p^\pm = \pm \frac{\Lambda(y)}{2}(p^- - p^+). \tag{3.19}$$

Using a well-balanced scheme, in the spirit of [7, 8], we get, for any $n \in \mathbb{N}$, $i \in \mathbb{Z}$ and $k \in \{-K, \dots, K\}$,

$$p_{i,k}^{+,n+1} = p_{i,k}^{+,n+\frac{1}{2}} - \frac{\Delta t}{\Delta x}(p_{i,k}^{+,n+\frac{1}{2}} - p_{i,k}^{-,n+\frac{1}{2}}) + \frac{\Delta t}{\Delta x(1+\frac{1}{2}\Lambda(y_k)\Delta x)}(p_{i-1,k}^{+,n+\frac{1}{2}} - p_{i,k}^{-,n+\frac{1}{2}}) \tag{3.20a}$$

$$p_{i-1,k}^{-,n+1} = p_{i-1,k}^{-,n+\frac{1}{2}} + \frac{\Delta t}{\Delta x}(p_{i-1,k}^{+,n+\frac{1}{2}} - p_{i-1,k}^{-,n+\frac{1}{2}}) + \frac{\Delta t}{\Delta x(1+\frac{1}{2}\Lambda(y_k)\Delta x)}(p_{i,k}^{-,n+\frac{1}{2}} - p_{i-1,k}^{+,n+\frac{1}{2}}). \tag{3.20b}$$

It is well-known that the numerical scheme (3.20) is stable and consistent with (3.19) provided a CFL condition is satisfied:

Lemma 3.1 *Let us assume that the following CFL condition $\Delta t \leq \Delta x$ holds and Λ is a nonnegative function. Then the scheme* (3.18)–(3.20) *is positive and conservative.*

Proof. Indeed, scheme (3.18) is clearly positive and conservative. For (3.20), it may be rewritten

$$p_{i,k}^{+,n+1} = p_{i,k}^{+,n+\frac{1}{2}}\left(1 - \frac{\Delta t}{\Delta x}\right) + \frac{\Delta t}{\Delta x}\left(1 - \frac{1}{1+\frac{1}{2}\Lambda(y_k)\Delta x}\right)p_{i,k}^{-,n+\frac{1}{2}} + \frac{\Delta t}{\Delta x(1+\frac{1}{2}\Lambda(y_k)\Delta x)}p_{i-1,k}^{+,n+\frac{1}{2}}$$

$$p_{i-1,k}^{-,n+1} = p_{i-1,k}^{-,n+\frac{1}{2}}\left(1 - \frac{\Delta t}{\Delta x}\right) + \frac{\Delta t}{\Delta x}\left(1 - \frac{1}{1+\frac{1}{2}\Lambda(y_k)\Delta x}\right)p_{i-1,k}^{-,n+\frac{1}{2}} + \frac{\Delta t}{\Delta x(1+\frac{1}{2}\Lambda(y_k)\Delta x)}p_{i,k}^{-,n+\frac{1}{2}}.$$

Then, since Λ is nonnegative, it is clear that all coefficients are positive under the CFL condition. $\square$

3.2 Asymptotic limit

We verify the behaviour of the scheme when $\varepsilon \to 0$.

Lemma 3.2 *Let the sequence* $(p_{i,k}^{\pm,n+\frac{1}{2}})_{i,k,n}$ *be computed thanks to scheme* (3.18). *When* $\varepsilon \to 0$, *we have* $p_{i,k}^{\pm,n+\frac{1}{2}} \to \bar{p}_i^{\pm,n}\delta_{k=\pm K}$, *where* $\bar{p}_i^{\pm,n} = \sum_{k=-K}^{K} p_{i,k}^{\pm,n}$.

Moreover, the sequence $(\bar{p}_i^{\pm,n})_{i,k,n}$ *satisfies the numerical scheme*

$$\bar{p}_i^{+,n+1} = \bar{p}_i^{+,n} - \frac{\Delta t}{\Delta x}(\bar{p}_i^{+,n} - \bar{p}_i^{-,n}) + \frac{\Delta t}{\Delta x(1+\frac{1}{2}\Lambda(G)\Delta x)}\bar{p}_{i-1}^{+,n} - \frac{\Delta t}{\Delta x(1+\frac{1}{2}\Lambda(-G)\Delta x)}\bar{p}_i^{-,n}, \quad (3.21a)$$

$$\bar{p}_{i-1}^{-,n+1} = \bar{p}_{i-1}^{+,n} + \frac{\Delta t}{\Delta x}(\bar{p}_{i-1}^{+,n} - \bar{p}_{i-1}^{-,n}) + \frac{\Delta t}{\Delta x(1+\frac{1}{2}\Lambda(-G)\Delta x)}\bar{p}_i^{-,n} - \frac{\Delta t}{\Delta x(1+\frac{1}{2}\Lambda(G)\Delta x)}\bar{p}_{i-1}^{+,n}. \quad (3.21b)$$

This is a consistent discretization of the kinetic equation (3.17).

Proof. Letting $\varepsilon \to 0$ in (3.18a), we deduce that at the limit we have, for any $k \in \{-K, \dots, K\}$, $J_{i,k+\frac{1}{2}}^{\pm,n+\frac{1}{2}} = J_{i,k-\frac{1}{2}}^{\pm,n+\frac{1}{2}} = 0$, where the latter equality is a consequence of the no-flux boundary condition. Then, for any i, k, n, the limit satisfies

$$(\pm G - y_k)^+ p_{i,k}^{\pm,n+\frac{1}{2}} = (\pm G - y_{k+1})^- p_{i,k+1}^{\pm,n+\frac{1}{2}}.$$

If $G > 0$, we choose $k+1 = K$ and deduce that $0 = p_{i,K-1}^{+,n+\frac{1}{2}}$. By induction $0 = p_{i,k}^{+,n+\frac{1}{2}}$ for any $k \le K-1$. For $k = -K$, we deduce that $0 = p_{i,-K+1}^{-,n+\frac{1}{2}}$, by induction, $0 = p_{i,k}^{-,n+\frac{1}{2}}$ for any $k \ge -K$.

If $G < 0$, by taking $k+1 = K$, we get $0 = p_{i,K-1}^{-,n+\frac{1}{2}}$. By induction, we deduce $0 = p_{i,k}^{-,n+\frac{1}{2}}$ for any $k \in \{-K, \dots, K\}$. For $k = -K$, we get $0 = p_{i,-K+1}^{+,n+\frac{1}{2}}$. Hence, $0 = p_{i,k}^{+,n+\frac{1}{2}}$ for any $k \in \{-K, \dots, K\}$.

Moreover, summing over k the equation (3.18a), we deduce that $\sum_{k=-K}^{K} p_{i,k}^{\pm,n+\frac{1}{2}} = \sum_{k=-K}^{K} p_{i,k}^{\pm,n}$.

Hence, summing (3.20a) and (3.20b) over k, we obtain the scheme (3.21). In order to verify the consistency with the kinetic equation (3.17), we recall the expansion

$$\frac{1}{1+\frac{1}{2}\Lambda(\pm G)\Delta x} = 1 - \frac{1}{2}\Lambda(\pm G)\Delta x + o(\Delta x).$$

Injecting this expression into (3.21a), we obtain

$$\begin{aligned}\bar{p}_i^{+,n+1} &= \bar{p}_i^{+,n} - \frac{\Delta t}{\Delta x}\left(\bar{p}_i^{+,n} - \bar{p}_{i-1}^{+,n} + \frac{1}{2}\Lambda(G)\Delta x\bar{p}_{i-1}^{+,n} - \frac{1}{2}\Lambda(-G)\Delta x\bar{p}_i^{-,n} + o(\Delta x)\right)\\ &= \bar{p}_i^{+,n} - \frac{\Delta t}{\Delta x}(\bar{p}_i^{+,n} - \bar{p}_{i-1}^{+,n}) - \frac{\Delta t}{2}\big(\Lambda(G)\bar{p}_{i-1}^{+,n} - \Lambda(-G)\bar{p}_i^{-,n}\big) + o(\Delta t).\end{aligned}$$

This is consistent with the equation for f^+ in (3.17). We proceed in the same way with (3.21b). □

3.3 A remark on the extension of this latter scheme to the diffusive regime

In this subsection, we underline the importance of a careful use of the splitting approach to recover the good asymptotic limit. Indeed, a natural extension of the scheme used in previous section to the diffusive regime will not provide a consistent scheme at the diffusive limit. In order to justify this affirmation, let us consider the following numerical scheme:

- We use the same upwind scheme as above for a first time step (3.18a)–(3.18b).
- In the second step, we discretize by a uniform scheme the equation

$$\varepsilon^2 \partial_t p^\pm \pm \varepsilon \partial_x p^\pm = \pm \frac{\Lambda(y)}{2}(p^- - p^+).$$

Using an asymptotic preserving well-balanced scheme, in the spirit of [7, 8], we get

$$\begin{aligned} p_{i,k}^{+,n+1} &= p_{i,k}^{+,n+\frac{1}{2}} - \frac{\Delta t}{\varepsilon \Delta x}(p_{i,k}^{+,n+1} - p_{i,k}^{-,n+1}) \\ &\quad + \frac{\Delta t}{\Delta x(\varepsilon + \frac{1}{2}\Lambda(y_k)\Delta x)}(p_{i-1,k}^{+,n+\frac{1}{2}} - p_{i,k}^{-,n+\frac{1}{2}}) \end{aligned} \tag{3.22}$$

$$\begin{aligned} p_{i-1,k}^{-,n+1} &= p_{i-1,k}^{-,n+\frac{1}{2}} + \frac{\Delta t}{\varepsilon \Delta x}(p_{i-1,k}^{+,n+1} - p_{i-1,k}^{-,n+1}) \\ &\quad + \frac{\Delta t}{\Delta x(\varepsilon + \frac{1}{2}\Lambda(y_k)\Delta x)}(p_{i,k}^{-,n+\frac{1}{2}} - p_{i-1,k}^{+,n+\frac{1}{2}}). \end{aligned} \tag{3.23}$$

Since this scheme is uniformly accurate with respect to ε, we may pass to the limit $\varepsilon \to 0$. After straightforward computations, we get from (3.22)–(3.23)

$$\begin{aligned} p_{i,k}^{+,n+1} &= \frac{\varepsilon \Delta x + \Delta t}{\varepsilon \Delta x + 2\Delta t} A_{i-\frac{1}{2},k}^{n+\frac{1}{2}} + \frac{\Delta t}{\varepsilon \Delta x + 2\Delta t} B_{i+\frac{1}{2},k}^{n+\frac{1}{2}} \\ p_{i,k}^{-,n+1} &= \frac{\Delta t}{\varepsilon \Delta x + 2\Delta t} A_{i-\frac{1}{2},k}^{n+\frac{1}{2}} + \frac{\varepsilon \Delta x + \Delta t}{\varepsilon \Delta x + 2\Delta t} B_{i+\frac{1}{2},k}^{n+\frac{1}{2}} \\ A_{i-\frac{1}{2},k}^{n+\frac{1}{2}} &= p_{i,k}^{+,n+\frac{1}{2}} + \frac{\Delta t}{\Delta x(\varepsilon + \frac{1}{2}\Lambda(y_k)\Delta x)}(p_{i-1,k}^{+,n+\frac{1}{2}} - p_{i,k}^{-,n+\frac{1}{2}}) \\ B_{i+\frac{1}{2},k}^{n+\frac{1}{2}} &= p_{i,k}^{-,n+\frac{1}{2}} + \frac{\Delta t}{\Delta x(\varepsilon + \frac{1}{2}\Lambda(y_k)\Delta x)}(p_{i+1,k}^{-,n+\frac{1}{2}} - p_{i,k}^{+,n+\frac{1}{2}}). \end{aligned}$$

As a first observation, we notice that when $\varepsilon \to 0$, we have

$$\lim_{\varepsilon \to 0} p_{i,k}^{+,n+1} = \lim_{\varepsilon \to 0} \frac{1}{2}(A_{i-\frac{1}{2},k}^{n+\frac{1}{2}} + B_{i+\frac{1}{2},k}^{n+\frac{1}{2}}) = \lim_{\varepsilon \to 0} p_{i,k}^{-,n+1}.$$

We deduce that for any $n \in \mathbb{N}^*$, we have $\lim_{\varepsilon \to 0} p_{i,k}^{+,n} = \lim_{\varepsilon \to 0} p_{i,k}^{-,n}$.
Moreover, by adding the first two equalities in the above numerical scheme, we get

$$p_{i,k}^{+,n+1} + p_{i,k}^{-,n+1} = A_{i-\frac{1}{2},k}^{n+\frac{1}{2}} + B_{i+\frac{1}{2},k}^{n+\frac{1}{2}}$$

Let us define the macroscopic density $\rho_i^n := \sum_{k=-K}^{K}(p_{i,k}^{+,n} + p_{i,k}^{-,n})$. Then, we have clearly

$$\rho_i^{n+1} = \sum_{k=-K}^{K} \Big(A_{i-\frac{1}{2},k}^{n+\frac{1}{2}} + B_{i+\frac{1}{2},k}^{n+\frac{1}{2}} \Big).$$

We pass to the limit $\varepsilon \to 0$ in the latter numerical scheme. We recall that from Lemma 3.2 (ii), we have $p_{i,k}^{\pm,n+\frac{1}{2}} \to \bar{p}_i^{\pm,n}\delta_{k=\pm K}$ where $\bar{p}_i^{\pm,n} = \sum_{k=-K}^{K} p_{i,k}^{\pm,n}$. Hence, passing into the limit, we obtain

$$\begin{aligned} A_{i-\frac{1}{2},k}^{n+\frac{1}{2}} &\to \Big(\bar{p}_i^{+,n} + \frac{2\Delta t}{\Lambda(G)\Delta x^2}\bar{p}_{i-1}^{+,n}\Big)\delta_{k=K} - \frac{2\Delta t}{\Lambda(-G)\Delta x^2}\bar{p}_i^{-,n}\delta_{k=-K} \\ B_{i+\frac{1}{2},k}^{n+\frac{1}{2}} &\to \Big(\bar{p}_i^{-,n} + \frac{2\Delta t}{\Lambda(-G)\Delta x^2}\bar{p}_{i+1}^{-,n}\Big)\delta_{k=-K} - \frac{2\Delta t}{\Lambda(G)\Delta x^2}\bar{p}_i^{+,n}\delta_{k=K}. \end{aligned}$$

Summing over k, and denoting $\bar{\rho}_i^n = \lim_{\varepsilon\to 0} \rho_i^n$, we arrive to the limiting scheme

$$\bar{\rho}_i^{n+1} = \bar{\rho}_i^n + \frac{2\Delta t}{\Delta x^2}\left(\frac{1}{\Lambda(G)}(\bar{p}_{i-1}^{+,n} - \bar{p}_i^{+,n}) + \frac{1}{\Lambda(-G)}(\bar{p}_{i+1}^{-,n} - \bar{p}_i^{-,n})\right).$$

With the fact that $\bar{p}_i^{+,n} = \bar{p}_i^{-,n} = \frac{1}{2}\bar{\rho}_i^n$, we get

$$\bar{\rho}_i^{n+1} = \bar{\rho}_i^n + \frac{\Delta t}{\Delta x^2}\left(\frac{1}{\Lambda(G)}(\bar{\rho}_{i-1}^n - \bar{\rho}_i^n) + \frac{1}{\Lambda(-G)}(\bar{\rho}_{i+1}^n - \bar{\rho}_i^n)\right).$$

This latter scheme is obviously not consistent with the Keller-Segel equation (2.7).

4 Numerical results

4.1 Problem

In order to illustrate our theoretical results, we carry out numerical computations for the following problem. Let us consider the one dimensional space $x \in [0,1]$ with mirror boundary conditions,

$$p^+(t, x=0, y) = p^-(t, x=0, y), \qquad p^-(t, x=1, y) = p^+(t, x=1, y).$$

These boundary conditions impose that the net mass flux at the boundary is zero; i.e.,

$$J = \int_{\mathbb{R}} (p^+ - p^-) dy = 0, \qquad \text{at} \quad x = 0, 1.$$

As the initial condition, we consider

$$p^{\pm}(t=0, x, y) = \begin{cases} \frac{1}{G}, & |y| \le \frac{|G|}{2}, \\ 0, & |y| > \frac{|G|}{2}, \end{cases}$$

for any $x \in [0,1]$. Hereafter we only consider the case where $G > 0$.

For this problem, the steady state solutions in the diffusive and hyperbolic limits are explicitly calculated as below :

Steady state in the diffusive limit. Let us consider the Keller-Segel system (2.7), which is obtained in the continuum limit at the diffusive scaling. We first recall that this equation is conservative, implying that $\int_0^L \bar{p}_0(t,x)\,dx = M$ for all positive time t. The steady states verify

$$\partial_x\left(\frac{1}{\Lambda(0)}\partial_x \bar{p}_0 + G\bar{p}_0\frac{\Lambda'(0)}{\Lambda(0)^2}\right) = 0.$$

Since the flux in the diffusive scaling is given by (2.6), the no flux boundary conditions give

$$\partial_x \bar{p}_0 + G\bar{p}_0\frac{\Lambda'(0)}{\Lambda(0)} = 0.$$

By integrating the above equation and using the mass conservation, we obtain

$$\bar{p}_0(x) = \frac{G\Lambda'(0)M}{\Lambda(0)\left(1 - e^{-\frac{G\Lambda'(0)}{\Lambda(0)}L}\right)} e^{-\frac{G\Lambda'(0)}{\Lambda(0)}x}. \tag{4.24}$$

Steady state in the hyperbolic limit. For the two-stream kinetic equation in the hyperbolic limit (3.17), the steady state can be explicitly computed. Indeed, it should satisfy :

$$\partial_x f^{\pm} = \frac{1}{2}(\Lambda(-G)f^- - \Lambda(G)f^+), \tag{4.25}$$

complemented with no-flux boundary conditions. By subtracting the above equations, we obtain $\partial_x(f^+ - f^-) = 0$. Thus $f^+ - f^-$ is constant, which is 0 thanks to the no-flux boundary conditions. Therefore, $f^+ = f^- = f$, injecting into (4.25), it gives

$$\partial_x f = \frac{1}{2}(\Lambda(-G) - \Lambda(G))f.$$

Integrating,

$$f(x) = Ae^{\frac{1}{2}(\Lambda(-G)-\Lambda(G))x}.$$

The constant A is computed thanks to the conservation of the mass : $M = \int_0^L f(x)\,dx$. Finally, we have

$$f(x) = \frac{(\Lambda(-G) - \Lambda(G))M}{2(e^{\frac{1}{2}(\Lambda(-G)-\Lambda(G))L} - 1)} e^{\frac{1}{2}(\Lambda(-G)-\Lambda(G))x}. \tag{4.26}$$

4.2 Numerical results for scheme (2.10)–(2.11)

The asymptotic preserving (AP-diff) scheme (2.10)–(2.11) is implemented for the problem in Section 4.1. Although this scheme is implicit, it can be implemented very efficiently. The computational procedure is described in Appendix 1. We carry out the numerical computations for various values of λ_0 and illustrate the validity of the AP-diff scheme by comparing the numerical results to those obtained by a MC method, which is explained in Appendix 2, and the analytical solution (4.24). We also investigate the accuracy of the AP-diff scheme by comparing the numerical results for different mesh systems.

For the response function $\Lambda(y)$, we consider

$$\Lambda(y) = 1 - \chi \arctan(y), \tag{4.27}$$

where χ is the modulation amplitude. In the following computations, unless otherwise stated, the parameters $G = 1$ and $\chi = 0.5$ are fixed.

Figure 1 shows the time dynamics of population density ρ for different values of λ_0. In Figure 1(a) and 1(b), the results of the AP-diff scheme are compared with those obtained by the MC method.

Although the AP-diff scheme and MC method are different types of numerical methods, both methods provide consistent numerical results. The distributions in the internal state y obtained by the AP-diff and MC methods are also compared in Figure 2. It is seen that even for the distribution functions both results coincide with each other. We also observe that the y-profile becomes narrower and more symmetric as λ_0 increases. This observation is consistent with the asymptotic behavior for small $\varepsilon = \lambda_0^{-1}$, where we know that $p^{\pm}$ concentrate at $y = 0$ in the continuum limit, i.e. $p^{\pm}(t, x, y) \to p_0(t, x)\delta_{y=0}$ as $\varepsilon \to 0$ (see Section 2.1).

However, when ε is too small, MC method may not be implemented efficiently. Then in Figure 1(c), the result of the AP-diff scheme for $\lambda_0 = 10^8$ is compared with the KS equation (2.15), which is the continuum limit equation when $\varepsilon \to 0$ of the two stream kinetic model at diffusive scaling. Remarkably, this comparison illustrates the asymptotic preserving nature of the AP-diff scheme.

Furthermore, Table 1 shows the numerical accuracy of the AP-diff scheme for different values of λ_0. It is seen that the AP-diff scheme is uniformly accurate and efficient irrespective of the parameter value of λ_0. Even for the small mesh system $I = 50$, the maximum relative error of the population density ρ, i.e., the error in the norm L^∞ divided by the local population density, is estimated less than 0.1%.

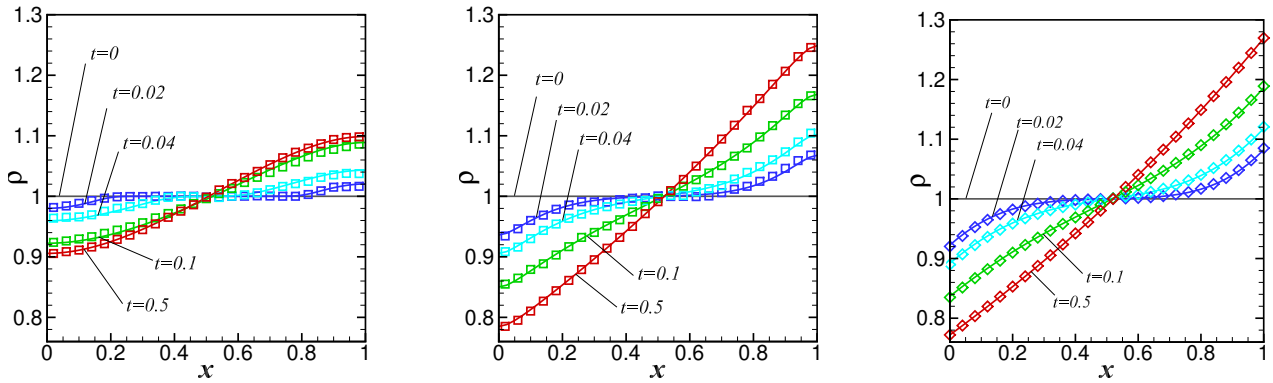

(a) (b) (c)

Figure 1: Time dynamics of ρ for different values of λ_0; i.e., $\lambda_0 = 10$ in (a), $\lambda_0 = 10^3$ in (b), and $\lambda_0 = 10^8$ in (c). The solid lines show the results obtained by the AP-diff scheme (2.10)– (2.11). The squared symbols show the results obtained by the MC method in (a) and (b) and those obtained by the finite-difference scheme of KS equation (2.15) in (c).

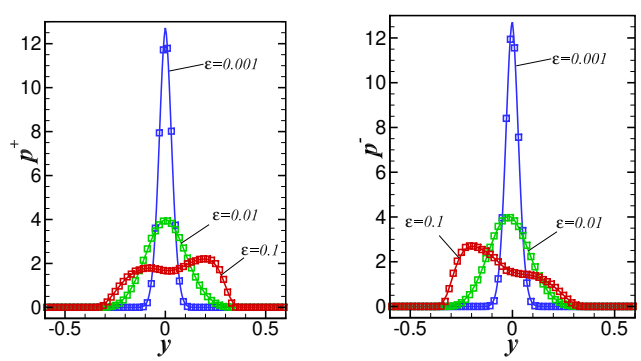

(a) (b)

Figure 2: Figures (a) and (b) show $p^+(y)$ and $p^-(y)$, respectively, for different values of $\varepsilon = \lambda_0^{-1}$. The solid lines show the results obtained by the AP-diff scheme while the plots with squared symbols show the results obtained by the MC method.

Table 1: Numerical accuracy of the AP-diff scheme for different values of λ_0. The maximum relative errors, i.e. the error in the norm L^∞ divided by the local population density, between the steady-state profiles of ρ obtained for two different mesh systems (I,I') are shown. The mesh size is set as Δx=Δy=$1/I$ and the time-step size is set as $\Delta t = 0.1\Delta x^2$. Read as 4.9e-4=4.9×10^{-4}

Mesh (I,I')	$\lambda_0 = 10$	$\lambda_0 = 10^2$	$\lambda_0 = 10^3$	$\lambda_0 = 10^8$
(50,200)	4.7e-4	6.7e-4	5.5e-4	4.1e-5
(100,200)	1.7e-4	2.4e-4	1.9e-4	8.1e-6

4.3 Numerical results for the second scheme (3.18)–(3.20)

In this Section, we consider the scheme (3.18)–(3.20), denoted AP-hyp scheme in the following, for the problem in Section 4.1 at the hyperbolic scaling (3.16). We carry out numerical computations for various values of τ and λ_0 and compare the results with those obtained by the MC method and the analytical solution in the limit $\tau \to 0$, (4.26).

Figure 3 displays the time dynamics of population density ρ for different values of τ when $\lambda_0 = 10$ is fixed. In each figure, the results obtained by the AP-hyp scheme are compared with those obtained by the MC method. It is clearly seen that the both methods can provide consistent results. Furthermore, in figure (c), the steady-state profiles obtained by the AP-hyp and MC schemes are compared with the analytical solution in the asymptotic limit $\tau \to 0$ (4.26). This comparison illustrate the validity of the AP-hyp scheme when $\tau \to 0$.

The distributions in the internal state y obtained by AP-hyp and MC methods are compared in Figure 4. It is seen that both methods can provide consistent results. It is also seen that the profile is completely different from that obtained at the diffusive scaling (see Fig. 2). As described in Section 3, in the hyperbolic scaling, the distribution functions $p^{\pm}$ concentrates at $y = \pm G$, respectively, when $\tau \to 0$. Figure 4 illustrates that the AP-hyp scheme reproduces this asymptotic behavior.

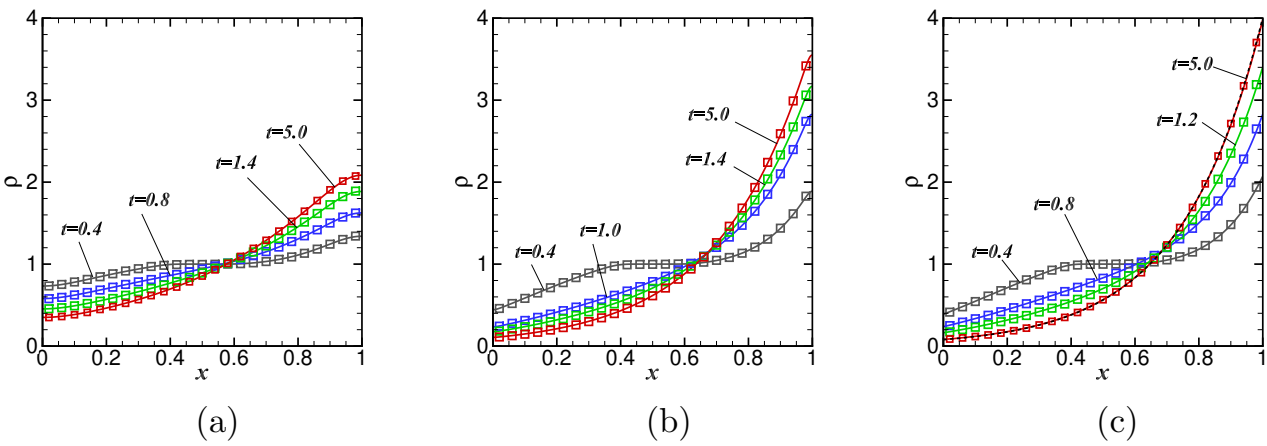

Figure 3: Time dynamics of ρ for different adaptation time τ; i.e., (a) τ=0.1, (b) τ=0.01 , and (c) $\tau = 10^{-8}$. The parameter $\lambda_0 = 10.0$ is fixed. The solid lines show the results obtained by the AP-hyp scheme while the squared symbols show those obtained by the MC method. In figure (c), the dashed line shows the analytical result in the limit $\tau \to 0$ calculated by Eq. (4.26).

Table 2 shows the numerical accuracy of the AP-hyp scheme. Compared with Table 1, it is seen that the AP-hyp scheme is less accurate than the AP-diff scheme for $\tau = 1$. However, the AP-hyp scheme keeps the accuracy even for a very small τ at $\lambda_0 = 10$.

When λ_0 is large, the accuracy of the AP-hyp scheme significantly falls at small values of τ. This is because the spatial profile of ρ becomes exponential for small values of τ when λ_0 is large. Indeed, the analytical solution for $\tau \to 0$ (4.26) indicates that the mass is concentrated at $x = 1$ when λ_0 is large. Figure 5 illustrates that the spatial profile of ρ becomes exponential when τ is small at $\lambda_0 = 100$. The growth rate is inversely proportional to τ.

4.4 Comparison of two schemes

In Section 4.2 we have implemented the AP-diff scheme for the two-stream kinetic system at diffusive scaling, where the parameter $\tau = 1$ is fixed. In this Section, in order to treat the variation of

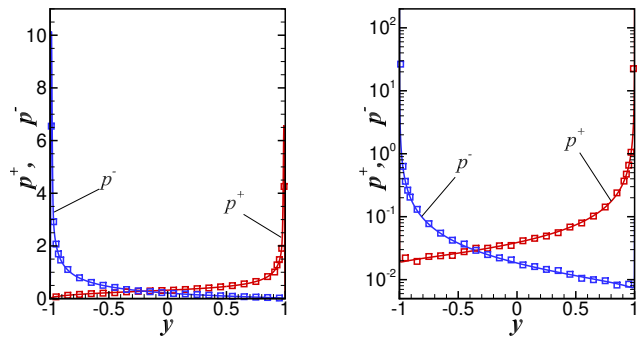

(a) (b)

Figure 4: Figures (a) and (b) show the results for τ=0.1 and τ=0.01, respectively. The parameters $\lambda_0 = 10$ is fixed. The solid lines show the results of the AP-hyp scheme while the symbols show the results of the MC method.

Table 2: Numerical accuracy of the AP-hyp scheme (3.18) and (3.20) for different values of τ at λ_0=10 and 100. The maximum relative errors, i.e. the error in the norm L^∞ divided by the local population density, between the spatial profiles of ρ obtained in two different mesh systems (I,I') are shown. The mesh size Δy is set as $\Delta y = \Delta x$. See also the caption in Table 1.

Mesh	$\lambda_0 = 10$				$\lambda_0 = 100$		
(I,I')	τ=1.0	τ=0.1	τ=0.01	τ=10^{-8}	$\tau = 1.0$	$\tau = 0.1$	τ=0.02
(200,800)	3.1e-3	2.0e-2	5.9e-2	5.6e-2	1.0e-2	1.0e-1	–
(400,800)	1.0e-3	6.7e-3	1.9e-2	1.9e-2	3.5e-3	3.4e-2	3.3e-1
(800,1600)	–	–	–	–	–	–	1.6e-1

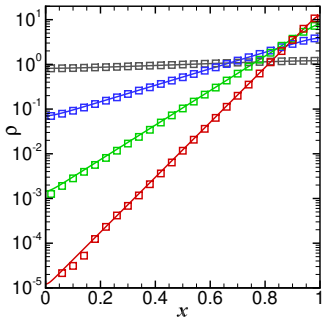

Figure 5: Spatial profiles of population density ρ for different values of τ. The parameter $\lambda_0 = 100$ is fixed. The solid lines show the results of the AP-hyp scheme and the symbols show the results of the MC method.

Table 3: Numerical accuracy of the AP-diff scheme for different values of τ at λ_0=10 and 100. The maximum relative errors between the spatial profiles of ρ obtained in two different mesh systems (I,I') are shown. The mesh size Δy is set as $\Delta y = \frac{|G|}{\tau}\Delta x$. See also the caption in Table 1.

Mesh	$\lambda_0 = 10$		$\lambda_0 = 100$	
(I,I')	$\tau = 0.1$	$\tau = 0.01$	$\tau = 0.1$	$\tau = 0.02$
(200,800)	8.9e-3	–	2.8e-2	–
(400,800)	3.0e-3	6.8e-2	9.4e-3	1.7e-1
(800,1600)	–	3.5e-3	–	8.6e-2

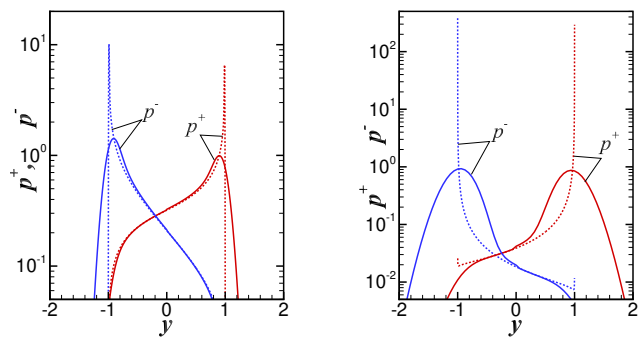

(a) (b)

Figure 6: Comparison of the y distribution obtained by the AP-diff scheme (solid lines) and that obtained by the hyperbolic scheme (dashed lines). Figure (a) and (b) show the results for $\tau = 0.1$ and $\tau = 0.01$, respectively, at $\lambda_0 = 10$.

parameter τ explicitely, we slightly modify the AP-diff scheme as following. We replace Δy with $\tau\Delta y$ in (2.10) and G with G/τ in (2.11) and (2.12). The relation between x- and y- mesh intervals is rewritten as $\Delta y = \frac{|G|}{\tau}\Delta x$ while the CFL condition (2.13) remains unchanged. Thus, when the parameter τ is small, the mesh size in y space, Δy becomes more coarsened than that in x space.

Although the diffusive scaling is not appropriate unless the parameter τ is sufficiently larger than λ_0^{-1}, we implement the modified AP-diff scheme for some small values of τ and investigate the applicability of the AP-diff scheme for small τ by comparing the results with those obtained by the AP-hyp scheme (3.18) and (3.20).

It should be noted that the AP-diff scheme is conservative when the condition $p^{\pm}_{i,K} = p^{\pm}_{i,-K} = 0$ for any $i \in \{0, \ldots, I\}$ is satisfied (see Appendix 3). Indeed, this condition is satisfied at the diffusive scaling since the internal state y is concentrated at $y = 0$ (See Fig. 2). However, as it is observed in Fig. 4, the internal state y is biased at $y = \pm G$ when τ is small. Thus, when we implement the modified AP-diff scheme for a small value of τ, we need to extend the domain of y in order to satisfy the mass conservation. In the following computations, we set the domain of y as $-3G \leq y \leq 3G$ for $\tau = 0.02$ and $-4G \leq y \leq 4G$ for $\tau = 0.01$ and divide the domain into the uniform mesh system with $\Delta y = \frac{|G|}{\tau}\Delta x$.

Table 3 shows the accuracy of the modified AP-diff method when the parameter τ varies. Compared to Table 2, it is found that the AP-diff scheme is more accurate than the AP-hyp scheme except for the case with $\tau = 0.01$ and $\lambda_0 = 10$. We also confirmed that the spatial profiles of ρ obtained by the AP-diff scheme and by the AP-hyp scheme coincide with each other within the numerical accuracy. Thus, these results confirm that the AP-diff scheme can accurately reproduce the macroscopic density ρ even for the case where the parameter τ is as small as λ_0^{-1}.

However, very interestingly, the distribution of the internal state y obtained by the AP-diff scheme is quite different from those obtained by the AP-hyp and MC methods. This illustrate the remark in Subsection 3.3. Figure 6 shows the distribution of the internal state y at $x = 0.5$ obtained by the AP scheme. The distribution of y obtained by the AP-hyp and MC methods for the same parameter values is shown in Fig. 2. In Figs. 6 (a) and (b), the results obtained by the AP-hyp scheme are also shown for comparison. The distributions of y obtained by the AP scheme also have peaks at $y = \pm G$. However, the profiles are much more diffusive than those obtained by the AP-hyp scheme.

5 Conclusion

This paper deals with the numerical discretization of a two-stream kinetic model for bacterial chemotaxis with internal state. We have proposed two schemes depending on the scaling parameters : AP-diff for the model at diffusive scaling, AP-hyp at hyperbolic scaling. Theses scheme have the property to be consistent with the asymptotic limit, which is the so-called asymptotic preserving property. In numerical parts, we implemented both AP-diff and AP-hyp schemes. Numerical convergence of the schemes is evaluated in detail by comparing the results obtained for different meshes. We also compare the numerical results obtained by the AP-diff and AP-hyp schemes to those obtained by a MC method and some analytical results in order to confirm the validity and consistency of the proposed schemes.

These numerical results confirm that the AP-diff scheme is uniformly accurate and efficient with respect to the variation of the tumbling frequency λ_0 at the diffusive scaling. From the comparisons between the AP-diff scheme and MC method, the consistency between the two methods is clearly observed. Remarkably, the asymptotic preserving nature of the AP-diff scheme is clearly illustrated by comparing the result obtained at a very small λ_0^{-1}, i.e., $\lambda_0^{-1} = 10^{-8}$, to the numerical solution of the KS equation.

The AP-hyp scheme is robust with respect to the variation of the parameter value τ. Even when the parameter τ is very small, i.e., $\tau = 10^{-8}$, the AP-hyp scheme can keep the numerical accuracy. The consistency of the AP-hyp scheme and MC method is also confirmed in the time dynamics of the macroscopic density and the distribution function of the internal sate at steady state.

Finally, we also compare the AP-diff scheme and the AP-hyp scheme after a slight modification of the original AP-diff scheme to treat the variation in τ. Although the AP-diff scheme loses the asymptotic preserving property when the parameter τ is comparable to or smaller than λ_0^{-1}, it accurately reproduces the macroscopic density for moderately small values of τ, where τ is still larger than λ_0^{-1}. However, interestingly, the distribution function of the internal state obtained by the AP-diff scheme is quite different from that obtained by the AP-hyp scheme and MC method for moderately small values of τ. This interesting observation illustrates the mismatch of the time splitting strategy and the asymptotic behavior of the solution. The importance of a careful strategy in the time splitting approach is discussed in detail in §3.3.

In summary, we conclude that the AP-diff scheme is very accurate and efficient at the diffusive scaling even in the continuum limit. Even when the parameter τ is moderately small, the AP-diff scheme can accurately reproduce the macroscopic density while it cannot reproduce the distribution function of the internal state. The AP-hyp scheme is valid in the variation of the parameter value τ. It can reproduce the hyperbolic limit behavior both in the macroscopic density and the distribution function of the internal state.

Acknowledgments

The authors would like to acknowledge partial funding from the Japan-France Integrated action Program PHC SAKURA, Grant number JPJSBP120193219.

References

[1] R. Bianchini, L. Gosse, A truly two-dimensional discretization of drift-diffusion equations on Cartesian grids, *SIAM J. Numer. Anal.* **56** 5, (2018), 2845–2870.

[2] Y. Dolak, C. Schmeiser, *Kinetic models for chemotaxis: Hydrodynamic limits and spatio-temporal mechanisms*, J. Math. Biol. 51 (2005), 595–615.

[3] R. Erban, H. Othmer, From individual to collective behaviour in bacterial chemotaxis, *SIAM J. Appl. Math.* **65**(2) (2004), 361–391.

[4] R. Erban, H. Othmer, Taxis equations for amoeboid cells, *J. Math. Biol.* (2007) **54**: 847–885.

[5] L. Gosse, *Computing Qualitatively Correct Approximations of Balance Laws*, vol. 2. Springer, Berlin (2013). ISBN 978-88-470-2891-3.

[6] L. Gosse, A well-balanced scheme able to cope with hydrodynamic limits for linear kinetic models, *Appl. Math. Lett.* **42** (2015), 15–21.

[7] L. Gosse, G. Toscani, An asymptotic preserving well-balanced scheme for the hyperbolic heat equation, *C.R. Acad. Sci. Paris Série I*, 334 (2002) 1-6.

[8] L. Gosse, N. Vauchelet, Some examples of kinetic schemes whose diffusion limit is Il'in's exponential-fitting, *Numer. Math.* **141** (2019), no 3, 627–680.

[9] L. Gosse, N. Vauchelet, A truly two-dimensional, asymptotic-preserving scheme for a discrete model of radiative transfer, *SIAM J. Numer. Anal.* (2020) 58 (2), 1092–1116.

[10] G. L. Hazelbauer, Bacterial chemotaxis: the early years of molecular studies, *Annu. Rev. Microbiol.* (2012) **66**: 285–303.

[11] T. Hillen and K. Painter, Transport and anisotropic diffusion models for movement in oriented habitats, Dispersal, Individual Movement and Spatial Ecology: A mathematical perspective. Eds: M.A. Lewis, P. Maini, S. Petrowskii, Heidelberg, Springer, 2012, 177–222.

[12] L. Jiang, Q. Ouyang, and Y. Tu, *Quantitative modeling of Escherichia coli chemotactic motion in environments varying in space and time*, PLoS Comput. Biol. 6 (2010), e1000735.

[13] S. Jin, Efficient asymptotic-preserving (AP) schemes for some multiscale kinetic equations, *SIAM J. Sci. Comput.* **21** (1999), 441–454.

[14] Y.V. Kalinin, L. Jiang, Y. Tu, M. Wu, Logarithmic sensing in Escherichia coli bacterial chemotaxis, *Biophys J* (2009) 96(6):2439–2448.

[15] H. Othmer, S. Dunbar, and W. Alt, *Models of dispersal in biological systems*, J. Math. Biol., 26 (1988), 263–298.

[16] H. G. Othmer, and T. Hillen, The diffusion limit of transport equations II: Chemotaxis equations, *SIAM J. Appl. Math.*, **62** (2002), 1222–1250.

[17] H.G. Othmer, X. Xin, C. Xue, Excitation and adaptation in bacteria-a model signal transduction system that controls taxis and spatial pattern formation. *Int J Mol Sci* (2013) 14(5):9205–9248.

[18] B. Perthame, M. Tang, N. Vauchelet, Derivation of a bacterial run-and-tumble kinetic equation from a model with biochemical pathway, *J. Math. Biol.* **73** (2016), no 5, 1161–1178.

[19] B. Perthame, W. Sun, M. Tang, S. Yasuda, Multiple asymptotics of kinetic equations with internal states, *Math. Models Methods Appl. Sci.* to appear.

[20] B. Perthame and S. Yasuda, Stiff-response-induced instability for chemotactic bacteria and flux-limited Keller-Segel equation, *Nonlinearity* **31** (2018), 4065–4089.

[21] G. Si, M. Tang, and X. Yang, A pathway-based mean-field model for E. coli chemo- taxis: mathematical derivation and keller-segel limit, *Multiscale Model Simul.* **12**(2), (2014), 907–926.

[22] G. Si, T. Wu, Q. Ouyang, and Y. Tu, A pathway-based mean-field model for Escherichia coli chemotaxis, *Phys. Rev. Lett.* **109** (2012), 048101.

[23] W. Sun, M. Tang, Macroscopic limits of pathway-based kinetic models for E. coli chemotaxis in large gradient environments, *Multiscale Model. Simul.* **15** (2017), no. 2, 797–826.

[24] Y. Tu, T.S. Shimizu, H.C. Berg, Modeling the chemotactic response of Escherichia coli to time-varying stimuli, *Proc Natl Acad Sci USA* (2008) 105(39): 14855–14860.

[25] C. Xue and H. G. Othmer. Multiscale models of taxis-driven patterning in bacterial populations, *SIAM J. Appl. Math.*, Vol. 70, no. 1,(2009), 133–167.

[26] C. Xue, Macroscopic equations for bacterial chemotaxis: integration of detailed biochemistry of cell signaling, *J. Math. Biol.*, Vol. 70, (2015), 1–44.

[27] S. Yasuda, Monte Carlo simulation for kinetic chemotaxis model: An application to the traveling population wave, *J. Comput. Phys.* **330** (2017), 1022–1042.

[28] X. Zhu, G. Si, N. Deng, Q. Ouyang, T. Wu, Z. He, L. Jiang, C. Luo, and Y. Tu, Frequency-dependent Escherichia coli chemotaxis behavior, *Phys. Rev. Lett.*, **108** (2012), 128101.

Appendix

1 Computational Procedure of the AP scheme

The well-balanced and asymptotic preserving (AP) scheme (2.10)-(2.12) is implemented efficiently by the following procedure. In the first step (2.10), $p_{i,k}^{\pm,n+\frac{1}{2}}$ for $k \in \{-K, \cdots, -1\}$ are calculated by using the only lower tridiagonal matrix as

$$p_{i,-K}^{\pm,n+\frac{1}{2}} = p_{i,-K}^{\pm,n} / \left(1 + \frac{\Delta t G}{\varepsilon \Delta y}\right),$$

and, for $k \in \{-K+1, \cdots, -1\}$,

$$p_{i,k}^{\pm,n+\frac{1}{2}} = \frac{\varepsilon \Delta y p_{i,k}^{\pm,n} - \Delta t y_{k-1} p_{i,k-1}^{\pm,n+\frac{1}{2}}}{\varepsilon \Delta y - \Delta t y_k}.$$

By the same token, $p_{i,k}^{\pm,n+\frac{1}{2}}$ for $k \in \{1, \cdots, K\}$ are calculated by using the only upper tridiagonal matrix. Then, $p_{i,0}^{\pm,n+\frac{1}{2}}$ is calculated as

$$p_{i,0}^{\pm,n+\frac{1}{2}} + \frac{\Delta t}{\varepsilon \Delta y}\left(y_1 p_{i,1}^{\pm,n+\frac{1}{2}} - y_{-1} p_{i,-1}^{\pm,n+\frac{1}{2}}\right) = p_{i,0}^{\pm,n}.$$

In the second step (2.11), by inverting the 2-by-2 matrix, we can explicitly calculate $p_{i,k}^{\pm,n+1}$ for $i \in \{1, \cdots, I-1\}$ and $k \in \{-K, \cdots, K\}$ from

$$\begin{aligned}\left(1 + \frac{2\Delta t}{\varepsilon \Delta x}\right) p_{i,k}^{+,n+1} = &\left(1 + \frac{\Delta t}{\varepsilon \Delta x}\right) p_{i,k}^{+,n+\frac{1}{2}} + \frac{\Delta t}{\varepsilon \Delta x} p_{i,k}^{-,n+\frac{1}{2}} \\ &+ \frac{2\Delta t(\Delta t + \varepsilon \Delta x) G}{\varepsilon \Delta x^2 (2\varepsilon G + \bar{\Lambda}_{k-\frac{1}{2}})}(p_{i-1,k-1}^{+,n+\frac{1}{2}} - p_{i,k}^{-,n+\frac{1}{2}}) \\ &+ \frac{2\Delta t^2 G}{\varepsilon \Delta x^2 (2\varepsilon G + \bar{\Lambda}_{k+\frac{1}{2}})}(p_{i+1,k+1}^{-,n+\frac{1}{2}} - p_{i,k}^{+,n+\frac{1}{2}}),\end{aligned}$$

and

$$\begin{aligned}\left(1 + \frac{2\Delta t}{\varepsilon \Delta x}\right) p_{i,k}^{-,n+1} = &\left(1 + \frac{\Delta t}{\varepsilon \Delta x}\right) p_{i,k}^{-,n+\frac{1}{2}} + \frac{\Delta t}{\varepsilon \Delta x} p_{i,k}^{+,n+\frac{1}{2}} \\ &+ \frac{2\Delta t^2 G}{\varepsilon \Delta x^2 (2\varepsilon G + \bar{\Lambda}_{k-\frac{1}{2}})}(p_{i-1,k-1}^{+,n+\frac{1}{2}} - p_{i,k}^{-,n+\frac{1}{2}}) \\ &+ \frac{2\Delta t(\Delta t + \varepsilon \Delta x) G}{\varepsilon \Delta x^2 (2\varepsilon G + \bar{\Lambda}_{k+\frac{1}{2}})}(p_{i+1,k+1}^{+,n+\frac{1}{2}} - p_{i,k}^{-,n+\frac{1}{2}}).\end{aligned}$$

Hereafter, we set $p_{i,K+1}^{\pm,n+\frac{1}{2}} = p_{i,-K-1}^{\pm,n+\frac{1}{2}} = 0$, which is equivalent with the non-flux condition $J_{i,K+\frac{1}{2}}^{\pm,n+\frac{1}{2}} = J_{i,-K-\frac{1}{2}}^{\pm,n+\frac{1}{2}} = 0$, for any i. By using the boundary conditions $p_{I,k}^{-,n+1} = p_{I,k}^{+,n+1}$ and $p_{0,k}^{+,n+1} = p_{0,k}^{-,n+1}$ in (2.11a) and (2.11b), respectively, we can compute

$$p_{I,k}^{+,n+1} = p_{I,k}^{+,n+\frac{1}{2}} + \frac{2\Delta t G}{\Delta x (2\varepsilon G + \bar{\Lambda}_{k-\frac{1}{2}})}(p_{I-1,k-1}^{+,n+\frac{1}{2}} - p_{I,k}^{-,n+\frac{1}{2}}),$$

$$p_{0,k}^{-,n+1} = p_{0,k}^{-,n+\frac{1}{2}} + \frac{2\Delta t G}{\Delta x(2\varepsilon G + \bar{\Lambda}_{k+\frac{1}{2}})}(p_{1,k+1}^{-,n+\frac{1}{2}} - p_{0,k}^{+,n+\frac{1}{2}}),$$

for any k.

2 Monte Carlo Method

We have extended a Monte Carlo (MC) code of the classical velocity-jump kinetic equation proposed in [20, 27] to treat the internal state y. The procedure of the MC method is described below. Here, we consider (1.4) in one-dimensional space $x \in [0, 1]$ and the same boundary condition in (4.1).

1. The initial states of each MC particle, i.e., the position $x_{(\ell)}^0$, velocity $v_{(\ell)}^0$, and internal state $y_{(\ell)}^0$ at the time step $n = 0$ are stochastically determined according to the initial distribution function $p^{\pm,0}(x, y)$. Hereafter, the superscript n represents the time step and the subscript ℓ represents the index of each MC particle.

2. Given the position, velocity, and internal state of the lth MC particle at time step n, the position and internal state of the MC particle is advanced in the time-step size Δt as

$$x_{(\ell)}^{n+1} = x_{(\ell)}^n + v_{(\ell)}^n \Delta t,$$

$$y_{(\ell)}^{n+1} = \frac{\tau y_{(\ell)}^n + \Delta t G v_{(\ell)}^n}{\tau + \Delta t}.$$

3. The particle which moves beyond the boundary at $x = 0$ (or $x = 1$), say the l'th particle at $x = x_{(\ell')}^{n+1} < 0$ (or $x = x_{(\ell')}^{n+1} > 1$), is relocated at $x = -x_{(\ell')}^{n+1}$ (or $x = 2 - x_{(\ell')}^{n+1}$) with changing the sign of the velocity as $v = -v_{(\ell')}^{n+1}$. This process corresponds to the no-flux boundary conditions.

4. Tumbling of each particle is decided by the probability $\lambda_0 \Lambda(y_{(\ell)}^{n+1})\Delta t/2$. The particles, which are decided to make tumble, change the sign of the velocities, $v_{(\ell)}^{n+1} = -v_{(\ell)}^n$, while other particles stay the velocities unchanged.

5. Return to the second process (2).

The macroscopic population density in each lattice site $x \in [i\Delta x, (i+1)\Delta x]$ $(i = 0, \cdots, I-1)$ is calculated as

$$\rho_i^n = \frac{1}{N_p \Delta x} \sum_{\ell=1}^{N_p} \int_{i\Delta x}^{(i+1)\Delta x} \delta(x - x_{(\ell)}^n) dx,$$

where N_p is the total particle number.

In §4, the time step size $\Delta t = 10^{-4}$ and the total particle number $N_p \simeq 1.2 \times 10^6$ are used except the cases for $\lambda_0 = 10^4$. For $\lambda_0 = 10^4$, we set $\Delta t = 1 \times 10^{-5}$.

3 Note on the mass conservation for the AP-diff scheme

In this part, we consider the mass conservation for the AP-diff scheme.

Lemma A.1 *Let us consider the AP-diff scheme* (2.10)–(2.11) *when* $G > 0$ *(the case* $G < 0$ *being similar) complemented with the no-flux boundary conditions* $J^{\pm,n+\frac{1}{2}}_{i,K+\frac{1}{2}} = J^{\pm,n+\frac{1}{2}}_{i,-K-\frac{1}{2}} = 0$ *which are equivalent to*

$$p^{\pm,n+\frac{1}{2}}_{i,K+1} = p^{\pm,n+\frac{1}{2}}_{i,-K-1} = 0, \tag{A.1}$$

and with reflection boundary conditions

$$p^{+,n}_{0,k} = p^{-,n}_{0,k}, \qquad p^{-,n}_{I,k} = p^{+,n}_{I,k}. \tag{A.2}$$

Then, if we assume moreover that $p^{+,n}_{i,K} = p^{-,n}_{i,-K} = 0$ *for any* $i \in \{0, \dots, I\}$*, we get that the AP-diff scheme is conservative.*

Proof. We define the local density by

$$\rho_i = \sum_{k=-K}^{K} \left(p^{+}_{i,k} + p^{-}_{i,k} \right)$$

and the total mass M, calculated by the trapezoidal law,

$$M = \frac{\rho_0 + \rho_I}{2} + \sum_{i=1}^{I-1} \rho_i.$$

Let $\bar{p}^{\pm,n}_i = \sum_{k=-K}^{K} p^{\pm,n}_{i,k}$, and $\bar{p}^{\pm,n+\frac{1}{2}}_i = \sum_{k=-K}^{K} p^{\pm,n+\frac{1}{2}}_{i,k}$, we obtain, from (2.10a) with the no-flux boundary conditions, $\bar{p}^{\pm,n+\frac{1}{2}}_i = \bar{p}^{\pm,n}_i$.

By summing up (2.11a) and (2.11b) w.r.t. k, we obtain, respectively,

$$\begin{aligned}
\bar{p}^{+,n+1}_i &= \bar{p}^{+,n+\frac{1}{2}}_i - \frac{\Delta t}{\varepsilon \Delta x} \left(\bar{p}^{+,n+1}_i - \bar{p}^{-,n+1}_i \right) + \sum_{k=-K}^{K} a_{k-\frac{1}{2}} \left(p^{+,n+\frac{1}{2}}_{i-1,k-1} - p^{-,n+\frac{1}{2}}_{i,k} \right) \\
&= \bar{p}^{+,n+\frac{1}{2}}_i - \frac{\Delta t}{\varepsilon \Delta x} \left(\bar{p}^{+,n+1}_i - \bar{p}^{-,n+1}_i \right) + \sum_{k=-K+1}^{K} a_{k-\frac{1}{2}} \left(p^{+,n+\frac{1}{2}}_{i-1,k-1} - p^{-,n+\frac{1}{2}}_{i,k} \right) \\
&\quad - a_{-K-\frac{1}{2}} p^{-,n+\frac{1}{2}}_{i,-K},
\end{aligned} \tag{A.3a}$$

where $a_{k-\frac{1}{2}} = \frac{2\Delta t G}{\Delta x (2\varepsilon G + \Lambda_{k-\frac{1}{2}})}$, and

$$\begin{aligned}
\bar{p}^{-,n+1}_i &= \bar{p}^{-,n+\frac{1}{2}}_i + \frac{\Delta t}{\varepsilon \Delta x} \left(\bar{p}^{+,n+1}_i - \bar{p}^{-,n+1}_i \right) + \sum_{k=-K}^{K} a_{k+\frac{1}{2}} \left(p^{-,n+\frac{1}{2}}_{i+1,k+1} - p^{+,n+\frac{1}{2}}_{i,k} \right), \\
&= \bar{p}^{-,n+\frac{1}{2}}_i + \frac{\Delta t}{\varepsilon \Delta x} \left(\bar{p}^{+,n+1}_i - \bar{p}^{-,n+1}_i \right) + \sum_{k=-K+1}^{K} a_{k-\frac{1}{2}} \left(p^{-,n+\frac{1}{2}}_{i+1,k} - p^{+,n+\frac{1}{2}}_{i,k-1} \right) \\
&\quad - a_{K+\frac{1}{2}} p^{+,n+\frac{1}{2}}_{i,K},
\end{aligned} \tag{A.3b}$$

where we use (A.1). Thus, by summing up the above equations, we have

$$\begin{aligned}
\rho^{n+1}_i = \rho^n_i &+ \sum_{k=-K+1}^{K} a_{k-\frac{1}{2}} \left(p^{+,n+\frac{1}{2}}_{i-1,k-1} - p^{+,n+\frac{1}{2}}_{i,k-1} + p^{-,n+\frac{1}{2}}_{i+1,k} - p^{-,n+\frac{1}{2}}_{i,k} \right) \\
&- a_{-K-\frac{1}{2}} p^{-,n+\frac{1}{2}}_{i,-K} - a_{K+\frac{1}{2}} p^{+,n+\frac{1}{2}}_{i,K},
\end{aligned}$$

and by further summing up for $i = 1$ to $i = I - 1$, we have

$$\sum_{i=1}^{I-1} \rho_i^{n+1} = \sum_{i=1}^{I-1} \rho_i^n + \sum_{k=-K+1}^{K} a_{k-\frac{1}{2}} \left(p_{0,k-1}^{+,n+\frac{1}{2}} - p_{I-1,k-1}^{+,n+\frac{1}{2}} + p_{I,k}^{-,n+\frac{1}{2}} - p_{1,k}^{-,n+\frac{1}{2}} \right) - \sum_{i=1}^{I-1} \left(a_{-K-\frac{1}{2}} p_{i,-K}^{-,n+\frac{1}{2}} + a_{K+\frac{1}{2}} p_{i,K}^{+,n+\frac{1}{2}} \right). \tag{A.4}$$

On the other hand, ρ_I and ρ_0 are calculated, respectively, from (A.3b) and (A.3a) as

$$\frac{\rho_I^{n+1}}{2} = \frac{\rho_I^n}{2} + \sum_{k=-K+1}^{K} a_{k-\frac{1}{2}} \left(p_{I-1,k-1}^{+,n+\frac{1}{2}} - p_{I,k}^{-,n+\frac{1}{2}} \right) - a_{-K-\frac{1}{2}} p_{I,-K}^{-,n+\frac{1}{2}}, \tag{A.5}$$

$$\frac{\rho_0^{n+1}}{2} = \frac{\rho_0^n}{2} + \sum_{k=-K+1}^{K} a_{k-\frac{1}{2}} \left(p_{1,k}^{-,n+\frac{1}{2}} - p_{0,k-1}^{+,n+\frac{1}{2}} \right) - a_{K+\frac{1}{2}} p_{0,K}^{+,n+\frac{1}{2}}, \tag{A.6}$$

where we use the reflection condition (A.2).

From (A.4)–(A.6), we obtain

$$M^{n+1} = M^n - \left(a_{-K-\frac{1}{2}} \sum_{i=1}^{I} p_{i,-K}^{-,n+\frac{1}{2}} + a_{K+\frac{1}{2}} \sum_{i=0}^{I-1} p_{i,K}^{+,n+\frac{1}{2}} \right).$$

Since $a_{k-\frac{1}{2}} > 0$, the condition for the mass conservation reads $p_{i,K}^{+,n} = p_{i,-K}^{-,n} = 0$, for any $i \in \{0, \ldots, I\}$. □